Intercalation of Alkali Metal into WTe_2, the Crystal Structure of $A_{0.5}WTe_2$ and Observation of a Metal-to-Semiconductor Transition

Patrick Schmidt,[a] Fabian Strauß,[b] Marcus Scheele,[b] Carl P. Romao,[c] Hans-Jürgen Meyer*[a]

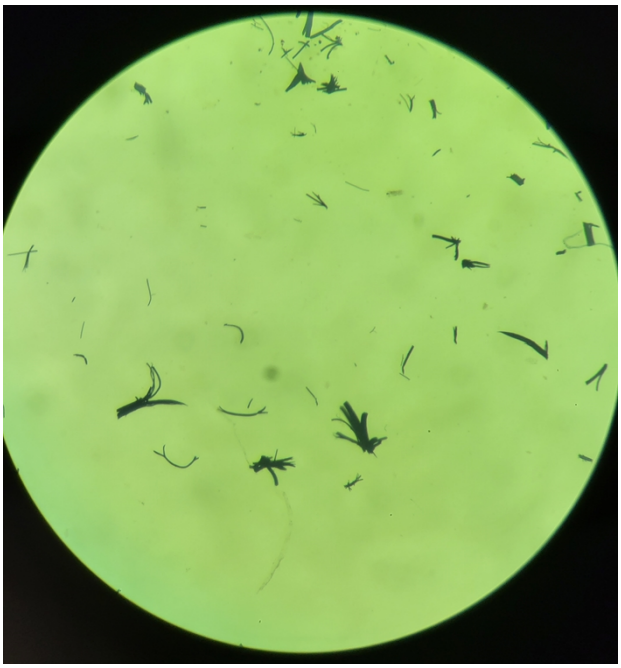

Figure S1. Microscope image (2x magnification) of WTe_2 single crystal in a 2 mM solution of rubidium naphthalenide after 30 min at room temperature.

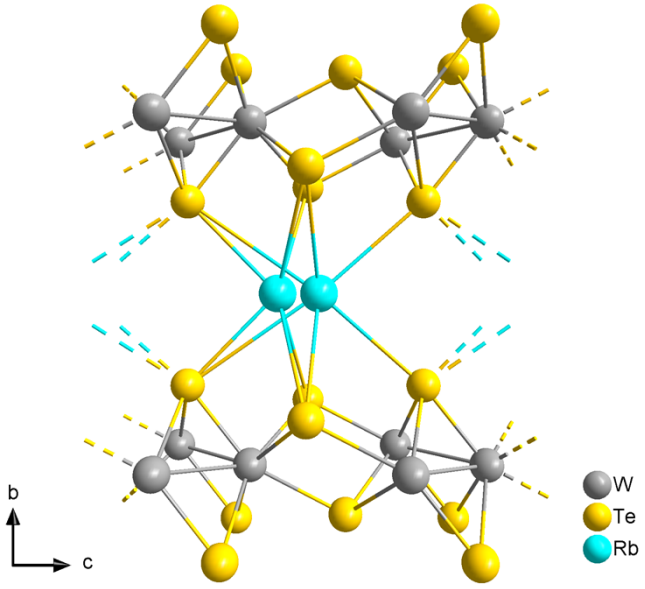

Figure S2. Section of the $Rb_{0.5}WTe_2$ initial structure solution of $Rb_{0.5}WTe_2$, showing two disordered rubidium positions with refined occupation factors close to 0.5.

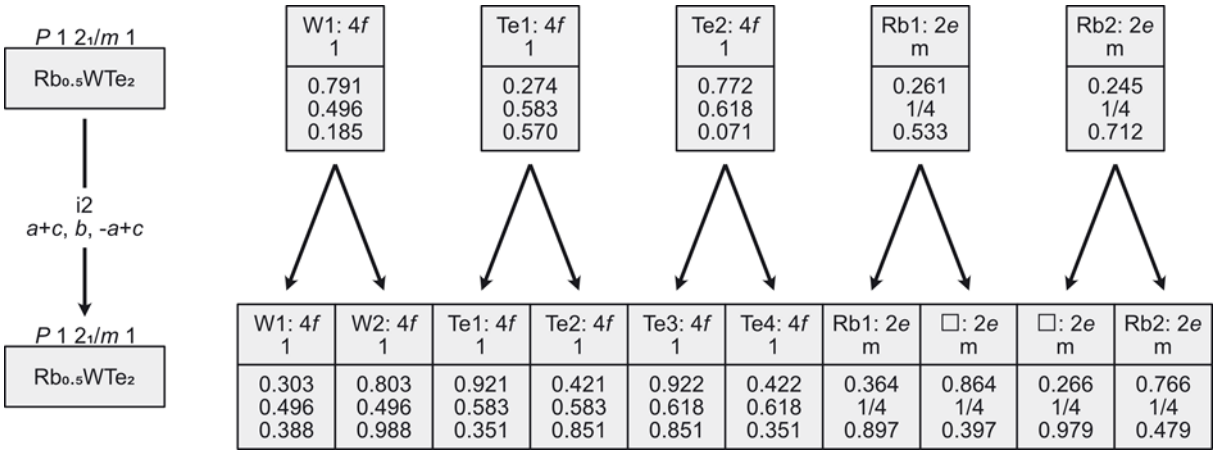

Figure S3. Bärnighausen tree: group-subgroup relation between the initial (top) and the final (bottom) structure solution of $Rb_{0.5}WTe_2$ with double cell volume and resolved disorder of the rubidium atoms.

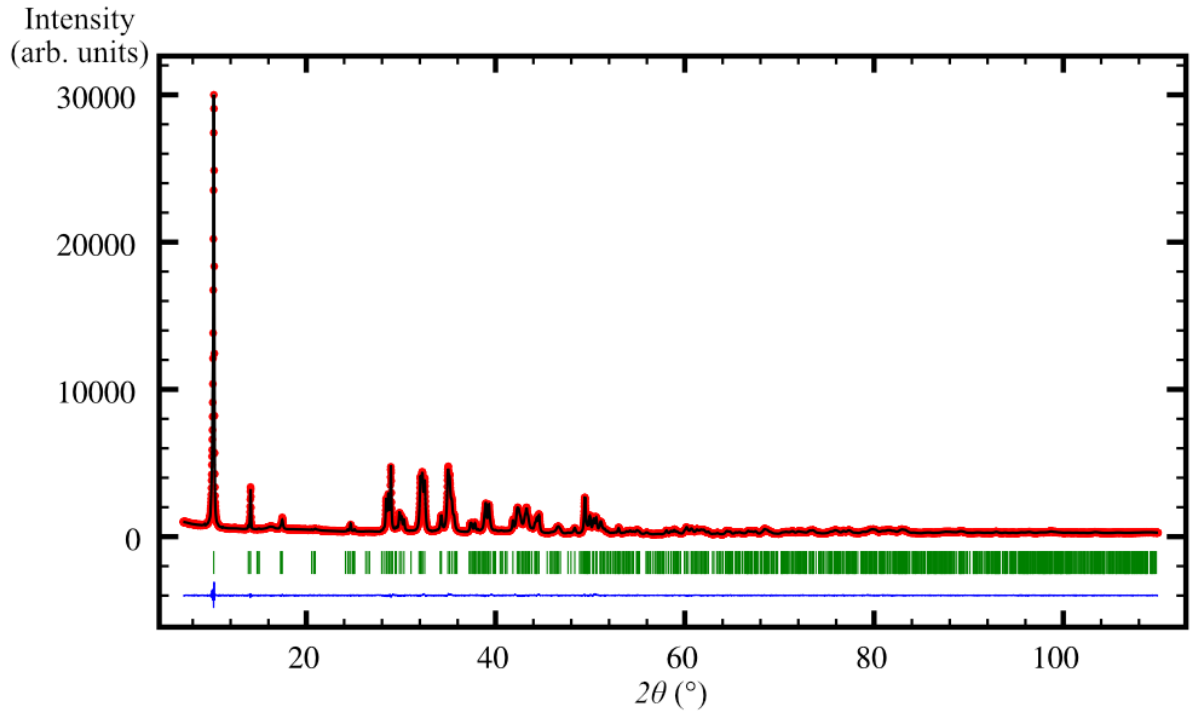

Figure S4. PXRD refinement of $K_{0.5}WTe_2$ at 298 K with the experimental (red) and calculated (black) intensities of the Rietveld refinement. Bragg positions (green) and the difference curve (blue) are also shown (CSD: 2392515).

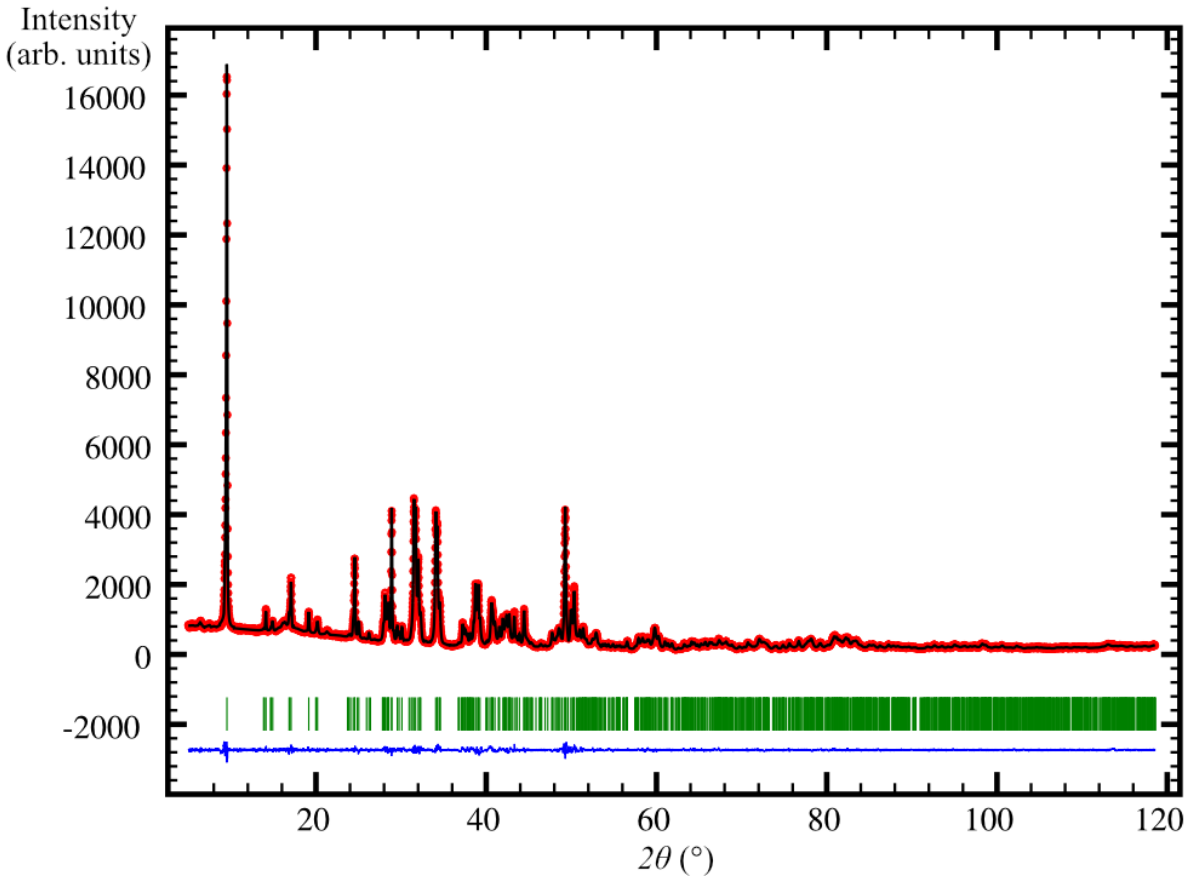

Figure S5. PXRD refinement of $Cs_{0.5}WTe_2$ at 298 K with the experimental (red) and calculated (black) intensities of the Rietveld refinement. Bragg positions (green) and the difference curve (blue) are also shown (CSD: 2390900).

Synthesis of $Li_{0.5}WTe_2$: $Li_{0.5}WTe_2$ was synthesized under an argon atmosphere by adding 10 mL of 2.5 M *n*-butyllithium (in hexane, Sigma-Aldrich) to 500 mg of WTe_2 (1.14 mmol) at room temperature. The mixture was gently agitated intermittently over five days. The solution was then decanted, and an additional 5 mL of 2.5 M *n*-butyllithium (in hexane) was added, followed by gentle shaking for another five days. After the reaction, the solution was removed, and the resulting solid was washed three times with 10 mL portions of absolute pentane. The final product was obtained as a black powder with a yield of ~95%.

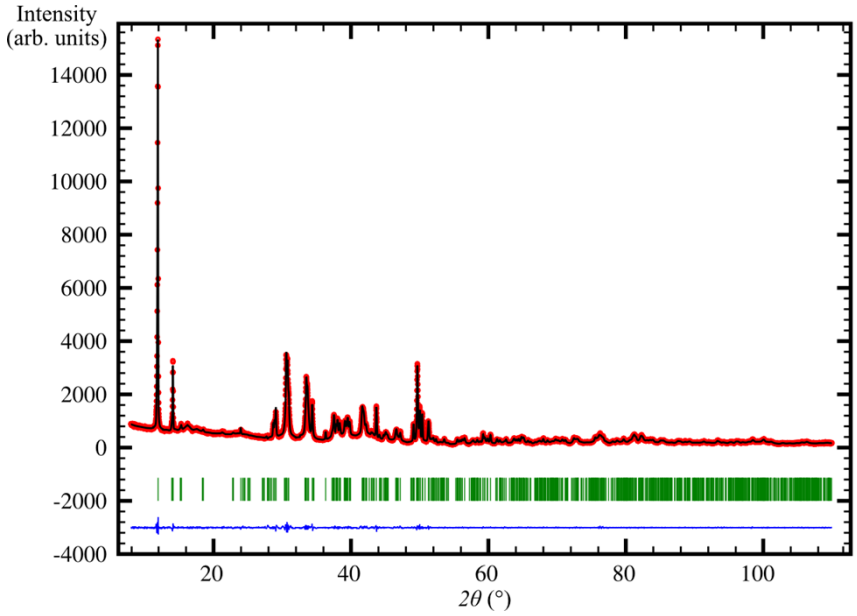

Figure S6. Le Bail profile fit to the PXRD pattern of $Li_{0.5}WTe_2$. Shown are the observed (red) and calculated (black) profiles, the difference curve (blue), and Bragg reflection positions (green). Refinement in the monoclinic space group $P2_1$ yields a = 7.28855(6) Å, b = 14.8297(2) Å, c = 7.23983(6) Å, and β = 119.3451(5)°.

Synthesis of $Na_{0.5}WTe_2$: $Na_{0.5}WTe_2$ was prepared using the same procedure as described for $A_{0.5}WTe_2$ (A = K, Rb, Cs) in the main text, employing sodium metal (99.95%, Sigma-Aldrich) as the alkali source. The reaction yielded a mixture of partially intercalated material with an overall yield of ~95%.

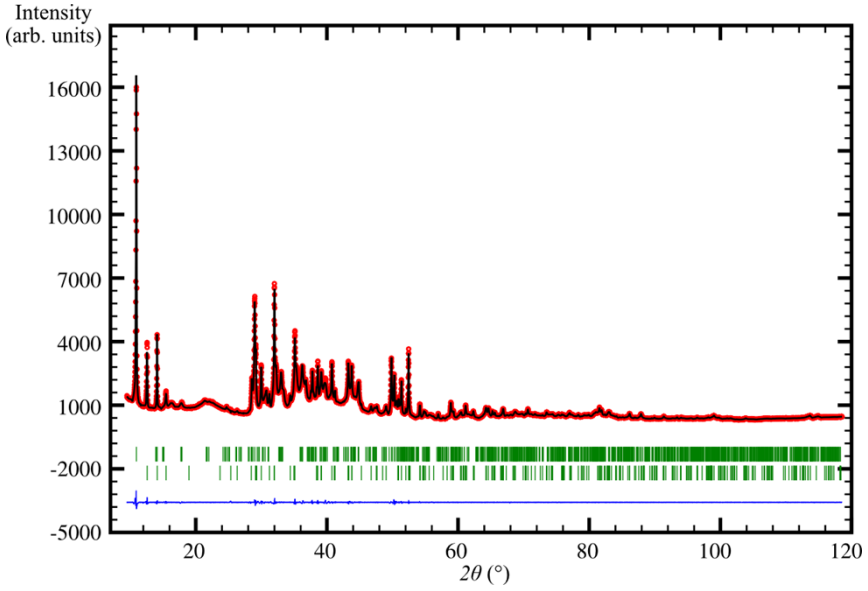

Figure S7. Le Bail profile fit to the PXRD pattern of $Na_{0.5}WTe_2$. Shown are the observed (red) and calculated (black) profiles, the difference curve (blue), and Bragg reflection positions (green, top= $Na_{0.5}WTe_2$, bottom=WTe_2). Refinement in the monoclinic space group $P2_1/m$ yields a = 7.2897(2) Å, b = 16.1501(3) Å, c = 7.24837(2) Å, and β = 119.1634(5)°. The pattern also contains ~30 mol% WTe_2 as an impurity.

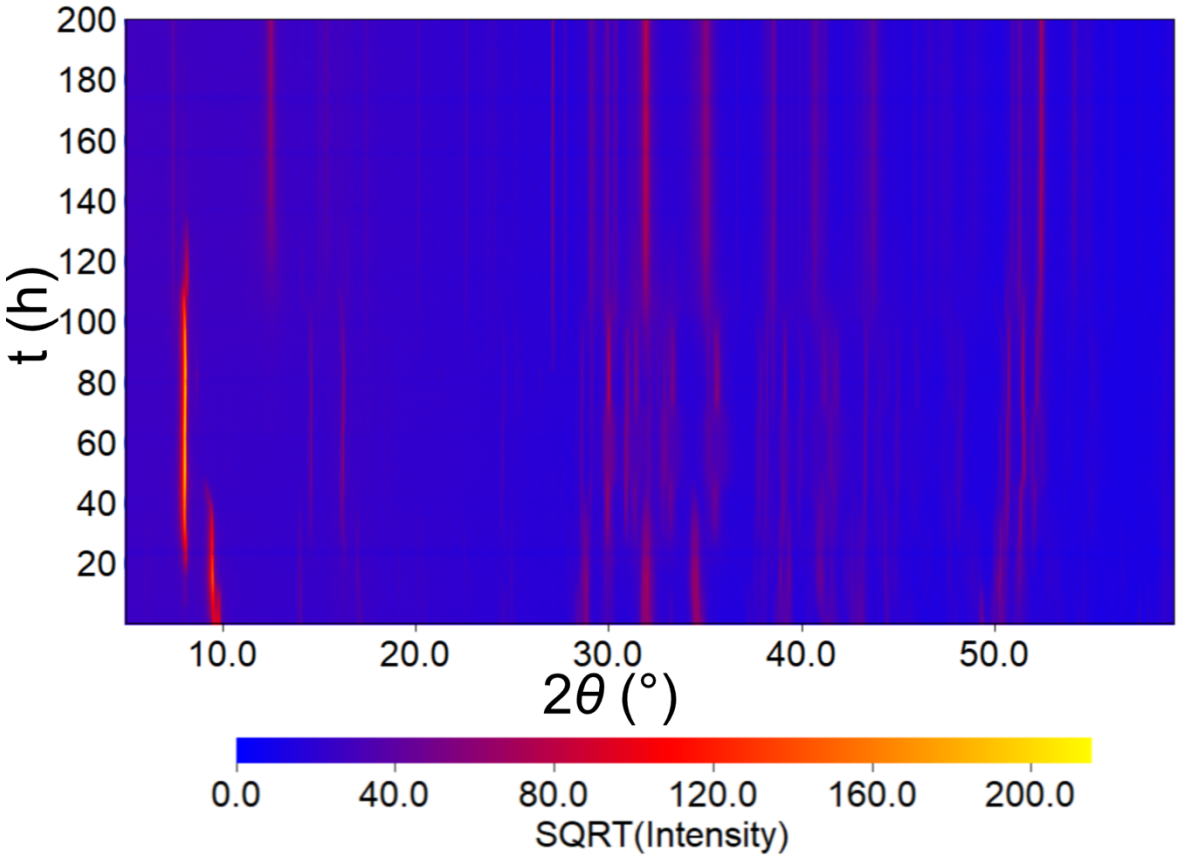

Figure S8. Time resolved PXRD analysis of $Rb_{0.5}WTe_2$ showing structural evolution upon exposure to ambient conditions. Note: Sample was mounted between two Mylar foils and was not hermetically sealed with Lithelen grease).

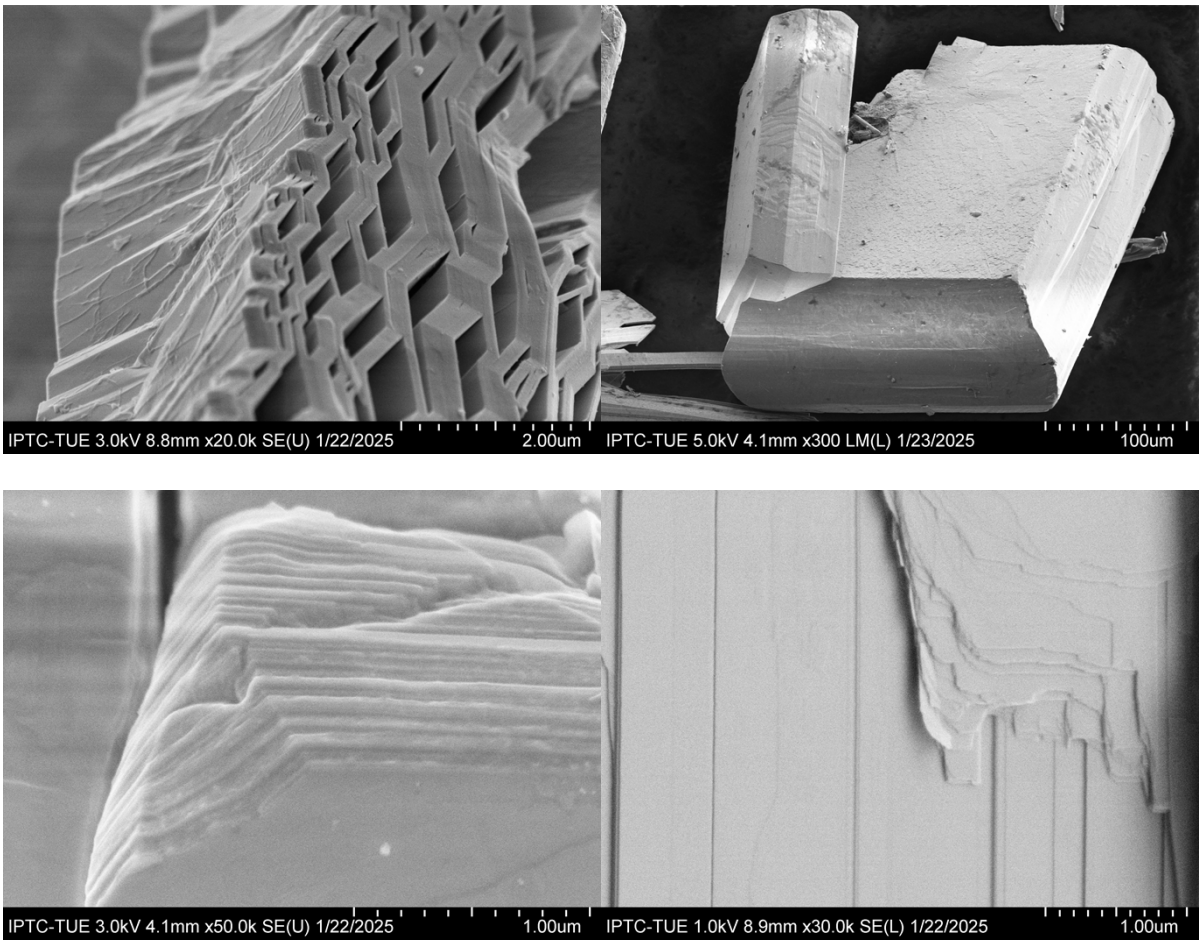

Figure S9. SEM images, highlighting the layered morphology of $Rb_{0.5}WTe_2$ crystals.

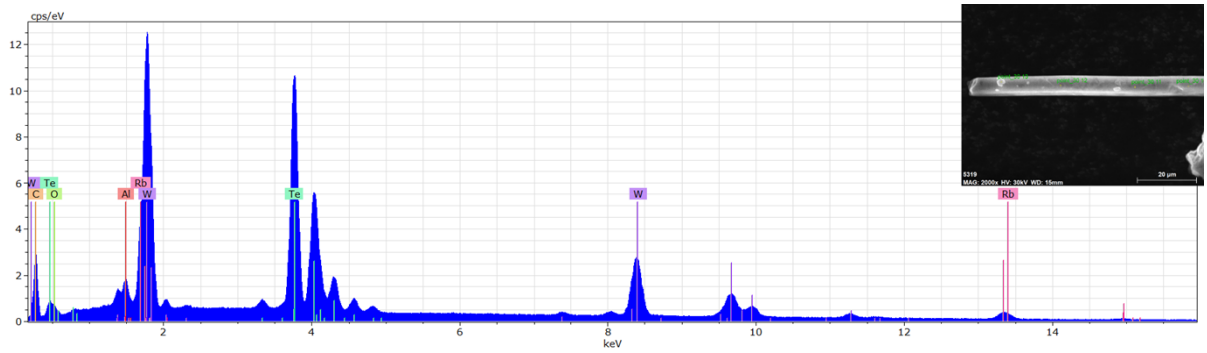

Figure S10. EDX spectra of $Rb_{0.5}WTe_2$, confirming the elemental composition and successful intercalation of rubidium. The inset SEM image indicates the precise measurement location, ensuring correlation between morphological features and compositional analysis. The presence of carbon and oxygen signals originates from the carbon tape used for sample mounting.

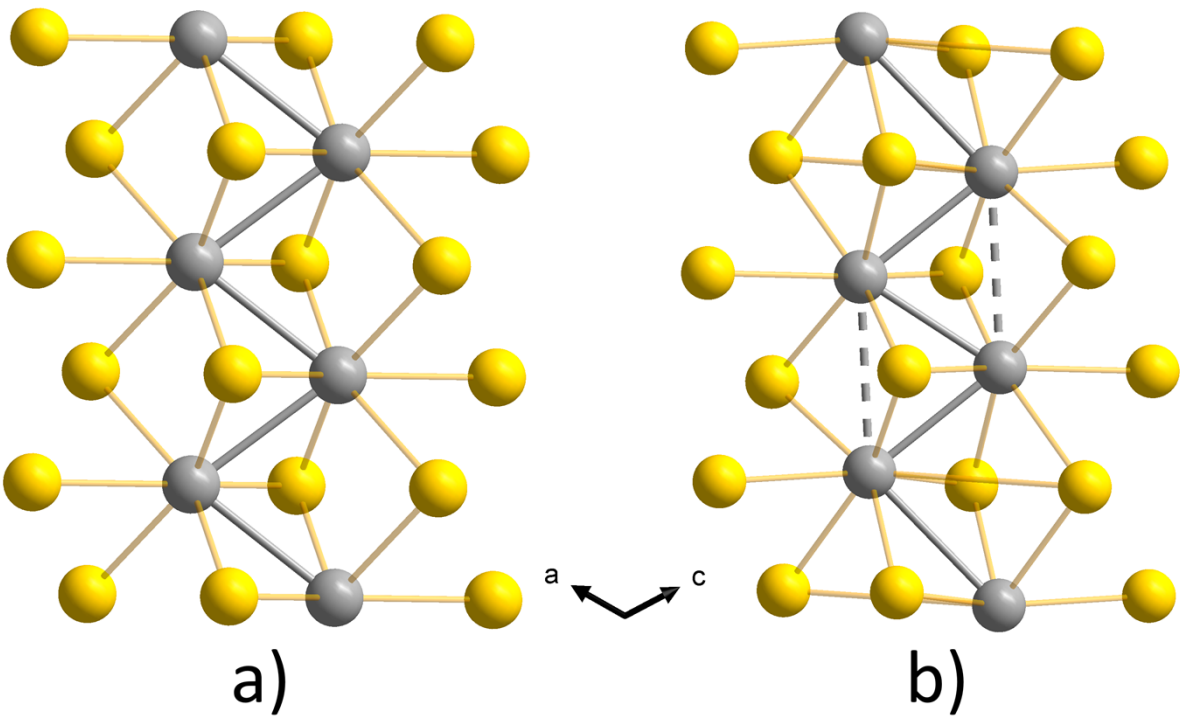

Figure S11. Local structural arrangement within a single layer of WTe_2 from DFT calculations in the $P2_1/m$ space group, showing the crystal structure without intercalating cations in (a) the neutral state and (b) with a −4 charge per unit cell (viewed along the *b*-axis; W: grey, Te: yellow). W_4 cluster formation is highlighted by dotted lines.

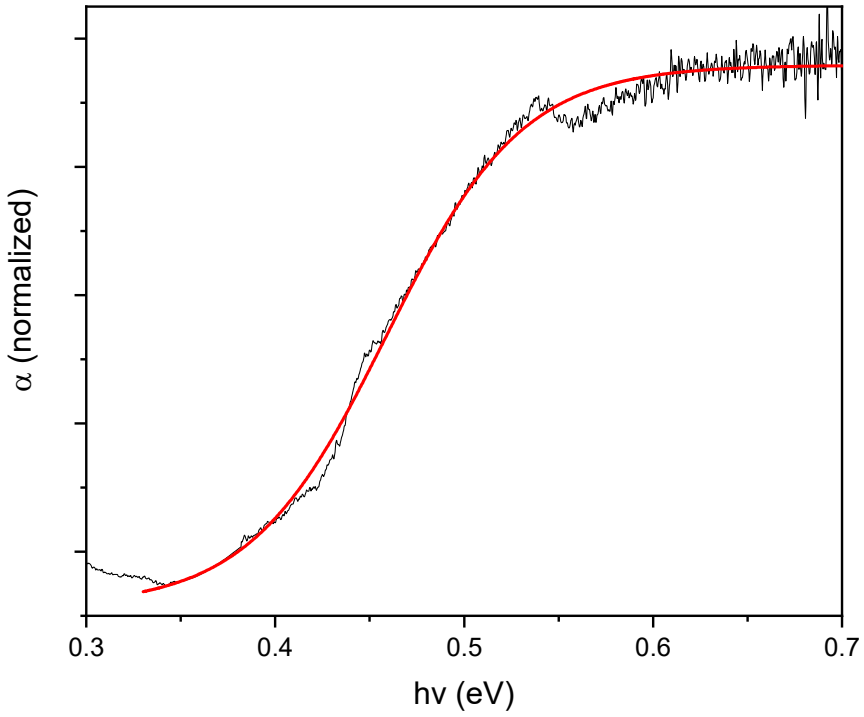

Figure S12. Optical absorption coefficient spectra of $Rb_{0.5}WTe_2$ with the Boltzmann function (R^2 = 0.995, $\chi^2 = 4.68 \cdot 10^{-3}$) used to fit $\alpha(normalized)$ with $E_{Boltz} = 0.4589(3)$ and dE = 0.03596(3).

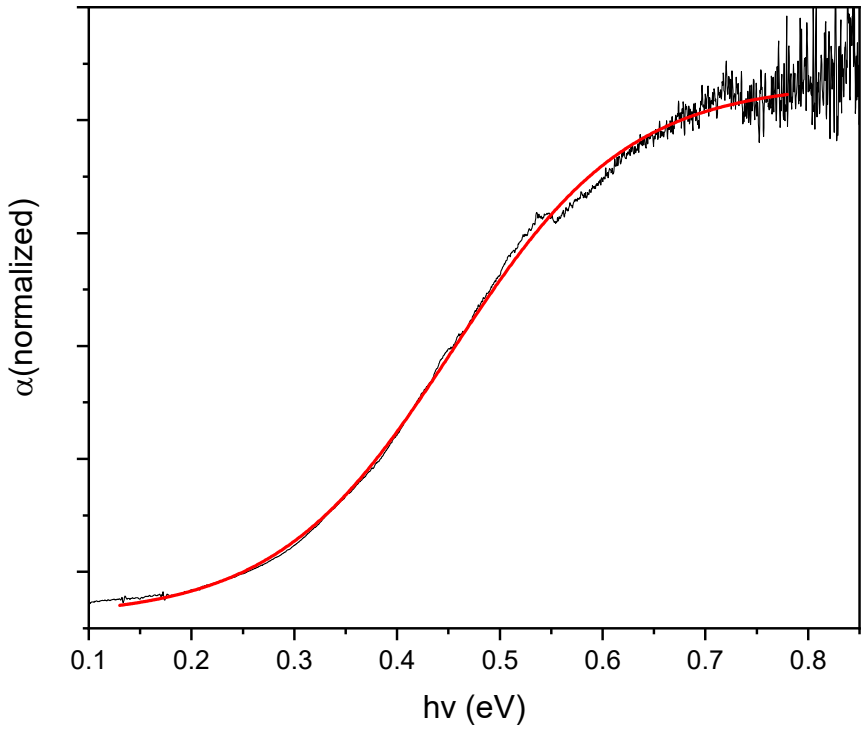

Figure S13. Optical absorption coefficient spectra of $Cs_{0.5}WTe_2$ with the Boltzmann function (R^2 = 0.997, χ^2 = 5.93·10^{-3}) used to fit $\alpha(normalized)$ with $E_{Boltz} = 0.4542(3)$ and dE = 0.0859(3).

Inert Chamber attachment for Harrick Praying Mantis Standard Sample Holder

All sample preparations were conducted under inert conditions (argon). The standard preparation procedure for DRIFT samples, including necessary adjustments, was followed. The measuring window was prepared by pressing a standard 13 mm press tool with 150 to 200 mg of KBr. The window was then fixed on top of the brass inert chamber attachment using vacuum-dried LVO 810 Lithelen grease, which was dried at 80 °C for a minimum of three days. After assembling the brass part with the sample holder, the pressure regulation hole was filled with grease to ensure a proper seal.

Although the KBr window degraded over time and was no longer intact for further measurements, the enclosed samples remained stable for at least one week when exposed to air.

Figure S14. Images of the brass inert chamber attachment (left) and the fully assembled setup (right), including the sample holder, KBr window, and sealing grease.

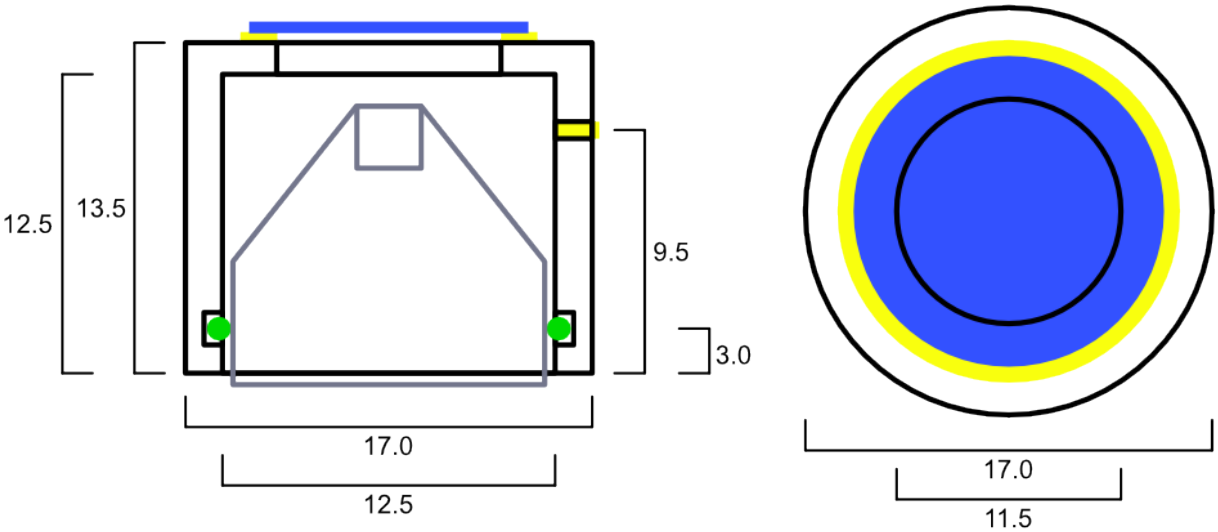

Figure S15. Schematic representation and dimensions (in mm) of the brass inert chamber attachment (black). The KBr window is shown in blue, sealing grease in yellow, rubber sealing ring in green, and the sample holder in grey.

Table S1: Interlayer spacing of pristine WTe_2 and its alkali-metal–intercalated derivatives, determined from PXRD via the (0 0 2) Bragg reflection.

Compound	Spacing / Å
WTe_2	7.009
$Li_{0.5}WTe_2$	7.4149
$Na_{0.5}WTe_2$	8.0751
$K_{0.5}WTe_2$	8.6297
$Rb_{0.5}WTe_2$	8.9179
$Cs_{0.5}WTe_2$	9.2606

Table S2: Atomic coordinates and equivalent isotropic displacement parameters (pm^2) for $K_{0.5}WTe_2$. U(eq) is defined as one third of the trace of the orthogonalized Uij tensor.

	x	*y*	*z*	*U*(eq)	SOF
W1	0.7404(3)	0.9941(2)	0.5669(3)	0.0261(2)	1
W2	0.80081(3)	0.00456(2)	0.98707(3)	0.0261(2)	1
Te1	0.582850(6)	0.076680(2)	0.178032(6)	0.02639(2)	1
Te2	0.07637(5)	0.08472(2)	0.65191(5)	0.02639(2)	1
Te3	0.569649(5)	0.110430(2)	0.682741(5)	0.02639(2)	1
Te4	0.07680(6)	0.12008(2)	0.14999(5)	0.02639(2)	1
K1	0.77796(2)	0.25	0.48274(2)	0.0234(2)	1
K2	0.36313(2)	0.25	0.8934(2)	0.0234(2)	1

Table S3: Atomic coordinates and equivalent isotropic displacement parameters (pm^2) for $Rb_{0.5}WTe_2$. U(eq) is defined as one third of the trace of the orthogonalized Uij tensor.

	x	*y*	*z*	*U*(eq)	SOF
W1	0.8033(3)	0.4963(3)	0.9879(3)	0.0254(3)	1
W2	0.7395(3)	0.5056(2)	0.5680(3)	0.0254(3)	1
Te1	0.9213(5)	0.5832(2)	0.3514(6)	0.0269(3)	1
Te2	0.5876(6)	0.4259(2)	0.1810(6)	0.0269(3)	1
Te3	0.9216(6)	0.6175(2)	0.8506(6)	0.0269(3)	1
Te4	0.5689(5)	0.3918(2)	0.6800(6)	0.0269(3)	1
Rb1	0.36435(9)	0.25	0.89691(9)	0.03674(1)	1
Rb2	0.7664(1)	0.25	0.47853(9)	0.03674(1)	1

Table S4: Atomic coordinates and equivalent isotropic displacement parameters (pm^2) for $Cs_{0.5}WTe_2$. U(eq) is defined as one third of the trace of the orthogonalized Uij tensor.

	x	*y*	*z*	*U*(eq)	SOF
W1	0.8036(3)	0.4964(2)	0.9880(3)	0.0183(2)	1
W2	0.7421(3)	0.50674(18)	0.5698(3)	0.0183(2)	1
Te1	0.9277(5)	0.5776(2)	0.3559(5)	0.0219(3)	1
Te2	0.5844(6)	0.4283(2)	0.1851(6)	0.0219(3)	1
Te3	0.9238(5)	0.6129(2)	0.8464(5)	0.0219(3)	1
Te4	0.5717(5)	0.3978(2)	0.6804(6)	0.0219(3)	1
Cs1	0.3697(6)	0.25	0.9041(6)	0.0310(2)	1
Cs2	0.7741(6)	0.25	0.4824(6)	0.0310(2)	1